



Cite this: DOI: 10.1039/c5ee01398d

Received 6th May 2015,
Accepted 2nd July 2015

DOI: 10.1039/c5ee01398d

www.rsc.org/ees

Achieving overall water splitting using titanium dioxide-based photocatalysts of different phases†

Rengui Li,^a Yuxiang Weng,^b Xin Zhou,^a Xiuli Wang,^a Yang Mi,^{bc} Ruifeng Chong,^{ac} Hongxian Han^a and Can Li^{*a}

Titanium dioxide (TiO₂) is regarded as the benchmark semiconductor in photocatalysis, which possesses a suitable band structure and makes the overall water splitting reaction thermodynamically possible. However, photocatalytic overall water splitting (POWS) (2H₂O → 2H₂ + O₂) can only take place on rutile but hardly on anatase and brookite TiO₂. So obtaining the POWS on TiO₂-based photocatalysts has remained a long-standing challenge for over 40 years. In this work, we found that the POWS on anatase and brookite TiO₂ becomes feasible under prolonged UV light irradiation. Further investigation by means of electron spin resonance spectroscopy (EPR) and transient infrared absorption–excitation energy scanning spectroscopy (TRIRA-ESS) reveals that both kinetics and thermodynamics factors contributed to unique POWS activity for different phases of TiO₂. Kinetically the process of photocatalysis differs on different phases of TiO₂ due to the intermediates (*OH radical for anatase and brookite TiO₂, peroxy species for rutile TiO₂) that are formed. Thermodynamically there are many trapped states lying near the valence band of anatase and brookite but not for rutile TiO₂, which reduce the overpotential for water oxidation. These findings develop our understanding of why some semiconductors are inactive as POWS photocatalysts despite having thermodynamically suitable band structures for the proton reduction and water oxidation reactions.

Solar hydrogen production using photocatalytic water splitting is regarded as a promising strategy for harnessing solar energy to supply hydrogen energy.^{1,2} Titanium dioxide (TiO₂) is a popular and standard semiconductor used in photocatalysis, and exists in three common crystalline structures, anatase, rutile and brookite, which have been extensively investigated. Generally, anatase TiO₂ is recognized as the most active phase in photocatalysts for

Broader context

Photocatalytic overall water splitting to produce H₂ is recognized as a promising strategy for utilization of solar energy. Titanium dioxide (TiO₂) has been widely used as the benchmark semiconductor in photocatalysis, which possesses a suitable band structure and makes the overall water splitting reaction thermodynamically possible. However, achieving overall water splitting on TiO₂-based photocatalysts has remained a long-standing challenge for over 40 years. In this work, we found that the overall water splitting can take place on all three phases of TiO₂ (anatase, rutile and brookite) after a prolonged UV light irradiation. Systematical investigations indicate that both kinetics and thermodynamics factors contributed to unique the photocatalytic overall water splitting activity for different phases of TiO₂. This finding will be helpful for understanding why many semiconductors are inactive as overall water splitting photocatalysts despite having thermodynamically suitable band structures for the proton reduction and water oxidation reactions.

environmental applications, while rutile and brookite TiO₂ are seldom considered.^{3–6} In the past few decades, almost all research studies on TiO₂ only showed H₂ but no O₂ was detected during photocatalytic overall water splitting although it has a thermodynamically feasible band structure. In the photocatalytic overall water splitting reaction (POWS, 2H₂O → 2H₂ + O₂), H₂ and O₂ should be produced simultaneously with a H₂/O₂ stoichiometric ratio of 2.0, which has been achieved in the photoelectrochemical (PEC) system using a TiO₂ photoanode as early as 1972.⁷ However, it has seldom been achieved on a TiO₂-based nanoparticle photocatalyst. This challenge persists despite the fact that TiO₂ has a suitable band structure for both proton reduction and water oxidation under UV light irradiation. Besides, a similar phenomenon has been observed for other popular photocatalysts (*e.g.*, Ta₃N₅, TaON). That is, some photocatalysts have suitable band structures that are thermodynamically feasible for POWS, yet they fail to catalyze the POWS reaction.

Immense efforts have been made to achieve POWS on TiO₂ previously. The introduction of some inorganic ions (*e.g.*, Cl[−], CO₃^{2−}) has been reported to somewhat improve the stoichiometric production of H₂ and O₂, which might be attributed to

^a State Key Laboratory of Catalysis, Dalian Institute of Chemical Physics, Chinese Academy of Sciences, Dalian National Laboratory for Clean Energy, Zhongshan Road 457, Dalian, 116023, China. E-mail: canli@dicp.ac.cn

^b The Key Laboratory of Softmatter Physics, The Institute of Physics, Chinese Academy of Sciences, Beijing 100190, China

^c University of Chinese Academy of Sciences, Beijing, 100049, China

† Electronic supplementary information (ESI) available. See DOI: 10.1039/c5ee01398d

the intermediates involving the ions (*e.g.*, $\text{C}_2\text{O}_4^{2-}$, ClO^-) that are formed in these systems.^{8,9} Recently, it was reported that the POWS can only take place on rutile but not on anatase TiO_2 .¹⁰ Nevertheless, the intrinsic reason for this observation remains unknown. In addition, the water splitting mechanism, especially the mechanism of water oxidation on TiO_2 -based photocatalysts are quite controversial in the literature.^{5,11–18}

Herein, we report our results that the photocatalytic overall water splitting (POWS) reaction can take place on TiO_2 -based photocatalysts with different phases (anatase, rutile and brookite) under prolonged UV light irradiation. We found that the stable overall water splitting with stoichiometric H_2/O_2 ratio can be achieved on rutile TiO_2 . However, anatase and brookite TiO_2 can only produce H_2 at the initial stage, but H_2 and O_2 are obtained simultaneously after long time irradiation. Further investigations using electron spin resonance spectroscopy (EPR), transient infrared absorption–excitation energy scanning spectroscopy (TRIRA-ESS) and DFT calculations reveal that both thermodynamics and kinetics contributed to the unique POWS activity for different phases of TiO_2 . Kinetically the process of photocatalysis differs on different phases of TiO_2 due to the intermediates ($\cdot\text{OH}$ radical for anatase and brookite TiO_2 , peroxy species for rutile TiO_2) that are formed. Thermodynamically there are many trapped states lying below the Fermi levels of anatase and brookite TiO_2 (but no trapped states can be found on rutile TiO_2), which can reduce the overpotential for water oxidation.

Theoretical calculation has demonstrated that the most stable surfaces of anatase and rutile TiO_2 are (101) and (110) facets.^{19,20} A similar calculation method was also introduced for brookite TiO_2 , which shows that the (210) facet is the most stable facet (Fig. S1 and Table S1, ESI†). Firstly, anatase, rutile and brookite TiO_2 samples exposed with (101), (110) and (210) facets were prepared according to the references.^{21,22} The as-prepared TiO_2 samples were demonstrated to be pure phases and well-crystallized by XRD and Raman characterization (Fig. 1a and b, Fig. S2, ESI†). HRTEM images revealed that the most exposed crystal facets for anatase, rutile and brookite TiO_2 samples are (101), (110) and (210), respectively, indicating that their stable surface structures are synthesized successfully (Fig. 1c–n).

Table 1 lists the POWS performance of the prepared different phases of TiO_2 samples under irradiation of a Xe lamp (the emission spectrum is shown in Fig. S3, ESI†). Only H_2 , but no O_2 , is detected for anatase TiO_2 indicating that the POWS reaction does not take place on the anatase TiO_2 (entries 1 and 2). However, both H_2 and O_2 are produced simultaneously on rutile TiO_2 with a H_2/O_2 ratio close to 2.0, indicating that the POWS ($2\text{H}_2\text{O} \rightarrow 2\text{H}_2 + \text{O}_2$) is achieved (entries 3, 4 and 5). In addition, brookite TiO_2 (entries 6) shows a similar performance to anatase TiO_2 , namely, only H_2 can be achieved but without any O_2 . Commercial TiO_2 samples were also investigated for comparison (entries 7 and 8). It can be found that only H_2 was produced for commercial anatase TiO_2 , however, commercial rutile can produce H_2 and O_2 simultaneously though the photoactivity is low. Similar results were also reported by using a series of commercial anatase and rutile TiO_2 from different supply corporations recently.²³

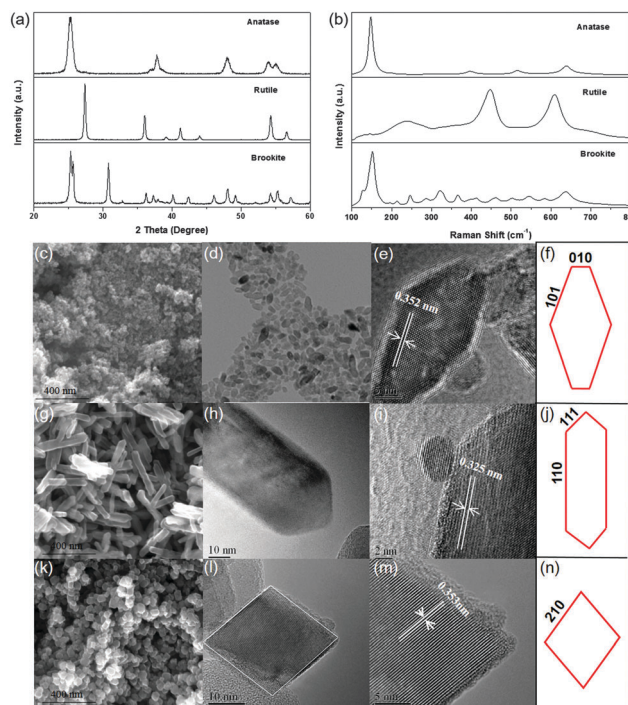


Fig. 1 (a) XRD patterns of the anatase, rutile and brookite TiO_2 ; (b) Raman spectra of the anatase, rutile and brookite TiO_2 ; (c–f) SEM and TEM images of anatase TiO_2 ; (g–j) SEM and TEM images of rutile TiO_2 ; (k–n) SEM and TEM images of brookite TiO_2 . A2, R3 and B1 samples in Table 1 were used in these characterizations.

Table 1 The photocatalytic water splitting of different phases of TiO_2 (anatase, rutile and brookite)

| Entry | Samples | Phase | Surface areas ($\text{m}^2 \text{g}^{-1}$) | The amount of gas evolution ($\mu\text{mol h}^{-1} \text{m}^2$) | | |
|-------|------------------|----------|--|---|--------------|-------------------------|
| | | | | H_2 | O_2 | H_2/O_2 |
| 1 | A1 | Anatase | 165.8 | 9.6 | 0 | — |
| 2 | A2 | Anatase | 152.5 | 10.5 | 0 | — |
| 3 | R1 | Rutile | 14.7 | 33.8 | 16.6 | 2.05 |
| 4 | R2 | Rutile | 19.2 | 23.5 | 11.5 | 2.04 |
| 5 | R3 | Rutile | 26.3 | 18.3 | 8.9 | 2.07 |
| 6 | B1 | Brookite | 26.2 | 24.8 | 0 | — |
| 7 | C-A ^a | Anatase | 52.6 | 6.3 | 0 | — |
| 8 | C-R ^a | Rutile | 23.4 | 4.2 | 2.1 | 2.04 |

Reaction conditions: photocatalyst, 50 mg; de-ionized H_2O , 150 mL; 0.2 wt% Pt was deposited by the *in situ* photo-deposition method; light source, xenon lamp (300 W); light intensity, 1000 mW cm^{-2} ; reaction vessel, top-irradiation type; reaction time, 1 h.^a C-A: commercial anatase; C-R: commercial rutile.

The above results clearly indicate that the POWS performance on the TiO_2 -based photocatalyst is closely related to its crystal-line phases.

The photocatalytic H_2 or O_2 production reaction in the presence of CH_3OH (holes acceptor) or AgNO_3 (electrons acceptor) was also performed to further evaluate the performances for TiO_2 samples (Fig. S4, ESI†). Anatase and brookite TiO_2 show comparable H_2 production performances, which is better than rutile TiO_2 in the presence of CH_3OH . However, rutile TiO_2 shows much better O_2 evolution performance than anatase and brookite TiO_2 .

when Ag^+ was used as an electron acceptor. The result shows the different reduction and oxidation ability for anatase, rutile and brookite TiO_2 , which led us to the conclusion that the POWS on TiO_2 is highly dependent on the crystalline phase of the TiO_2 , especially for the water oxidation reaction. This result also indicates that anatase and brookite TiO_2 exhibit similar performance both for H_2 production and O_2 production half reactions.

To investigate the photogenerated holes for anatase or brookite TiO_2 during the proton reduction for H_2 production, a photocatalytic experiment under prolonged UV light irradiation (light intensity, 1000 mW cm^{-2}) was carried out. As shown in Fig. 2a, only H_2 without O_2 is produced in the initial stage for anatase TiO_2 . In a subsequent experiment, the reaction system was then vacuumed and no O_2 was detected, but the H_2 production rate decreased. In the second cycle, the H_2 production rate decreased and O_2 was still not detected. In the third cycle after the

whole reaction time of more than 5 hours, small amount of oxygen was detected and maintained in the following cycles. The appearance of O_2 evolution after sufficient light irradiation is a surprising result. Fig. 2b shows the results of rutile TiO_2 throughout several cycles of the reaction test. H_2 and O_2 production with a H_2/O_2 ratio close to 2.0 was always maintained. Interestingly, brookite TiO_2 shows a similar phenomenon to anatase TiO_2 (Fig. 2c), namely, H_2 was only produced at the initial stage but O_2 was generated simultaneously after prolonged UV light irradiation. The phenomenon that anatase and brookite TiO_2 show similar performances for the POWS reaction could be ascribed to the similar atomic structure between brookite(210) and anatase(101) facets.²⁴ It should be pointed out that all the samples in Table 1 were used in this experiment and the samples with the same phases show similar performance. These results clearly indicate that the POWS to produce both H_2 and O_2 can be achieved not only for rutile TiO_2 but also for anatase and brookite TiO_2 . Notably, we found that O_2 can be produced on anatase and brookite TiO_2 after prolonged UV irradiation during the photocatalytic reaction.

To understand why the different phases of TiO_2 perform differently as photocatalysts in the POWS reaction, we characterized major aspects of the issue, including carrier dynamics, kinetics and thermodynamics. Particularly, we focused on the differences in water oxidation for the different phases of TiO_2 .

The transient dynamics of the two commonly-used phases, anatase and rutile TiO_2 were studied to probe the lifetimes of photoexcited holes. The lifetimes of the holes excited in rutile TiO_2 were found to be longer than those in anatase TiO_2 . However, in the presence of a Pt cocatalyst, the lifetimes were almost the same for both anatase and rutile TiO_2 (shown in Fig. S5a, ESI†). It should be noted that the Pt was deposited as a cocatalyst in all the POWS reactions for both anatase and rutile TiO_2 (without the Pt cocatalyst, no H_2 evolution is detected for either the anatase or rutile TiO_2). Thus, the dynamics of the photogenerated holes in the anatase and rutile TiO_2 are quite similar. To further clarify this point, Ag^+ (AgNO_3) was introduced as an electron acceptor to investigate the behavior of the photoexcited holes, and again the lifetimes of the photoexcited holes were almost the same, indicating that the dynamics of the photogenerated holes for anatase and rutile TiO_2 are similar. Therefore, we can conclude that the initial dynamics of photogenerated holes are not responsible for the behaviors of the different phases of TiO_2 in POWS.

To further explore the different oxygen-containing intermediates on different phases of TiO_2 we employed the EPR spin-trap technique to probe the reactive oxygen species derived on the surface of TiO_2 under UV light irradiation. Firstly, we performed the EPR experiment for all three TiO_2 samples with DMPO (dimethyl pyridine *N*-oxide) as an electron trapping agent under an atmosphere of Ar (Fig. 3). No signal was detected in the dark but totally different signals for three TiO_2 samples were obtained under light irradiation. For anatase TiO_2 , four characteristic peaks are obviously observed and the standard ratios of intensities are 1 : 2 : 2 : 1, which can be ascribed to $\cdot\text{DMPO-OH}$.^{13,17,25} In addition, brookite TiO_2 shows

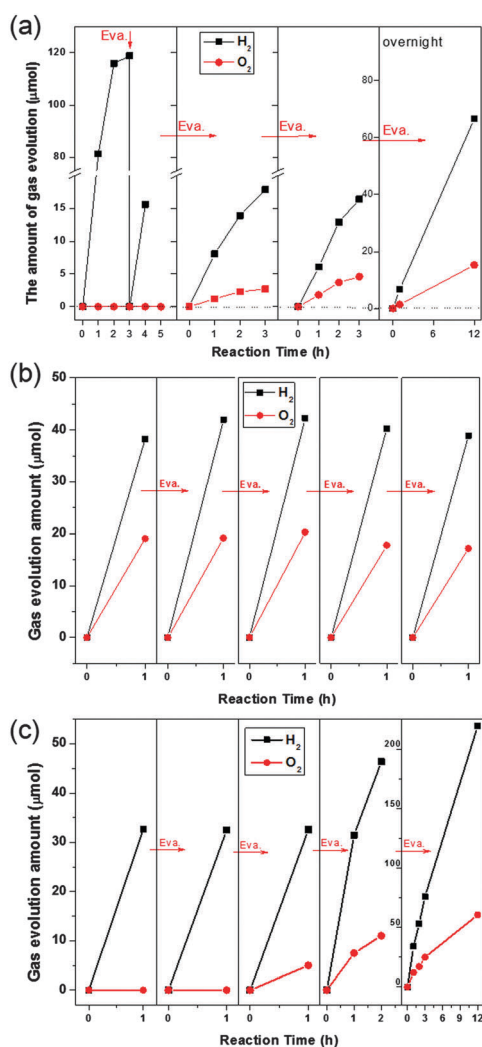


Fig. 2 The stability of photocatalytic water splitting for different phases of TiO_2 . (a) Anatase, (b) rutile and (c) brookite. Reaction conditions: photocatalyst, 50 mg; de-ionized H_2O , 150 mL; cocatalysts: 0.2 wt% Pt, photo-deposition method; light source, xenon lamp (300 W); light intensity, 1000 mW cm^{-2} ; reaction vessel, top-irradiation type. A2, R3 and B1 samples in Table 1 were used in these characterizations.

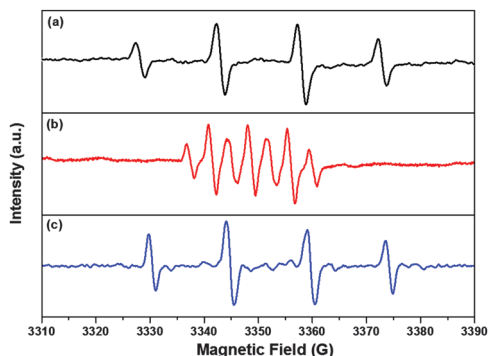


Fig. 3 Typical EPR spectra for photocatalytic oxidation of H_2O on different phases of TiO_2 in the presence of DMPO as an electron trapping agent. (a) Anatase TiO_2 , (b) rutile TiO_2 and (c) brookite TiO_2 . The signals were collected under light irradiation. Without light irradiation, no signal was detected. Conditions: TiO_2 concentrations, 0.1 mg mL^{-1} ; DMPO, 5 mM, in argon; irradiation time, 5 min; test temperature, 298 K; light source: 100 W Hg lamp, the distance between the sample and the light source was fixed at 1.0 m; irradiation time, 5 min. Instrumental settings: microwave power, 20 mW; modulation amplitude, 200 kHz; scan times, 10.

almost the same EPR signal with anatase TiO_2 , which is in good agreement with their similar photocatalytic performances. However, for rutile TiO_2 , a typical seven-line paramagnetic signal is detected, which can be ascribed to $\bullet\text{DMPO-X}$ as reported.^{26–28} We can infer that it is generated from the oxidation of DMPO by peroxide. It was also reported that peroxy species may serve as the reaction intermediates for the water oxidation on rutile TiO_2 .^{11–13} Valdes *et al.* reported that peroxy species can be easily decomposed to O_2 by DFT and concluded that this reaction step is the most favored step on rutile in the water oxidation reaction.¹⁸ So we can speculate that the peroxy species can be easily decomposed to produce O_2 on rutile. However, for anatase and brookite TiO_2 , the formed $\bullet\text{OH}$ radical may be strongly adsorbed on the surface and coupled to evolve O_2 after saturation of absorption. The different oxygen-containing intermediates formed on anatase and rutile TiO_2 can also be demonstrated by the diversity of surface hydroxyl oxygen of TiO_2 before and after the reaction^{29,30} (Fig. S6 and S7, ESI†). It was found that the proportion of hydroxyl oxygen for anatase TiO_2 is obviously increased after UV light irradiation (from 5.0% to 9.7%) but remained almost unchanged for rutile TiO_2 . Thus, the peroxy species are the most likely oxygen-containing intermediate derived from water oxidation on rutile TiO_2 while $\bullet\text{OH}$ radical species prefer to prevail from water oxidation on anatase TiO_2 . Our EPR results suggest that different intermediates are really formed during the photocatalytic water splitting for three kinds of TiO_2 samples (peroxy species for rutile TiO_2 , $\bullet\text{OH}$ radical for anatase and brookite TiO_2). The different intermediates resulted in different surface reaction processes, which mainly contribute to the kinetics for POWS on TiO_2 -based photocatalysts.

EPR experiments without electron trapping agents were also conducted under an Ar atmosphere. Fig. 4 shows the EPR results with and without UV light irradiation. The red-line signals were collected after 20 min UV light irradiation and

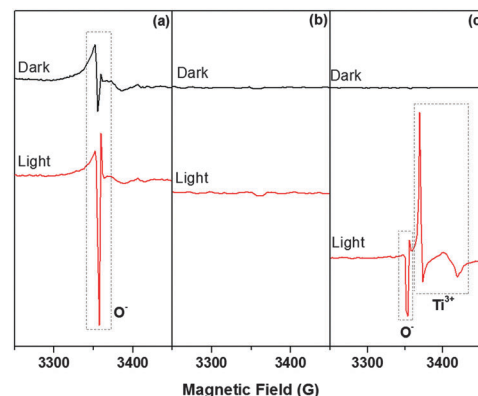


Fig. 4 Typical EPR spectra for photocatalytic oxidation of H_2O on different phases of TiO_2 with and without light irradiation. (a) Anatase TiO_2 , (b) rutile TiO_2 and (c) brookite TiO_2 . The signals were collected after 20 min irradiation. Conditions: 50 mg TiO_2 samples, in argon; test temperature, 100 K; light source: 100 W Hg lamp, the distance between sample and the light source was fixed to 1.0 m. Instrumental settings: microwave power, 20 mW; modulation amplitude, 200 kHz; scan times, 10.

then the sample tubes were quickly transferred for detection. No signals were detected for rutile TiO_2 regardless of dark conditions or light irradiation. However, anatase TiO_2 shows an obvious EPR signal at $g = 1.9998$, which could be ascribed to $\text{O}^{\bullet-}$.^{31,32} A weak signal at $g = 1.9890$ could be ascribed to the unsaturated Ti^{3+} .^{31,33,34} The signal of $\text{O}^{\bullet-}$ became stronger after UV light irradiation, indicating that part of O^{2-} in the lattice could be oxidized to $\text{O}^{\bullet-}$ by photoexcited holes during the photocatalytic reaction. For brookite TiO_2 , no signal was detected under dark conditions while a strong EPR signal at $g = 1.9998$, which is ascribed to $\text{O}^{\bullet-}$ similar to anatase TiO_2 . Interestingly, the signals at $g = 1.9890$ and $g = 1.9621$ were only achieved on brookite TiO_2 , which are ascribed to the unsaturated Ti^{3+} . The presence of Ti^{3+} under light irradiation most possibly contributes to the non-stoichiometric ratio of H_2/O_2 for anatase and brookite TiO_2 because partial photoexcited holes participate in the oxidation of the lattice oxygen to the observed $\text{O}^{\bullet-}$.

To further investigate the thermodynamics for different POWS performances on TiO_2 -based photocatalysts, different phases of TiO_2 were also characterized by the recently reported transient infrared absorption-excitation energy scanning spectroscopy (TRIRA-ESS), which can identify deep trapped electron energy levels above the valence band (VB) but below the Fermi level of the trapped electrons, the corresponding integrated density of the states, and the shallow trapping energy level below the conduction band.^{35,36} The TRIRA-ESS results shown in Fig. 5a can be divided into two regions: one below the Fermi-level of the trapped electrons (*i.e.*, from 0 to 1.79 eV) arising from the trapping states above the VB, and another region above the Fermi-level of the trapped electrons but below the conduction band (CB) originating from the shallow trapping states. There are remarkable differences between anatase and rutile TiO_2 in the region below the Fermi-level of the trapped electrons (denoted as E_{FS} , which is different from the Fermi level of free electrons in the

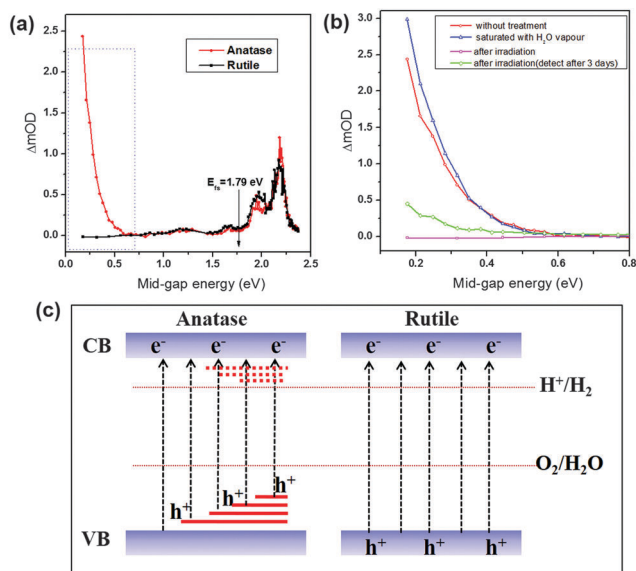


Fig. 5 (a) Typical transient IR absorption–excitation energy scanning spectra for anatase and rutile TiO₂. (b) TRIRA-EES for anatase TiO₂ under various conditions: (1) without any treatment; (2) saturated with water vapor; (3) pre-irradiation by 30 mW He–Cd laser (325 nm) for 3.5 hours; (4) pre-irradiation and then recovering for three days after laser treatment. (c) Energy diagram of the trapped electron states for anatase and rutile TiO₂.

CB denoted as E_{Fn}^{37}), namely, there are deep trapped states obviously observed in the anatase TiO₂ that are not present in the rutile TiO₂. The TRIRA-EES for brookite TiO₂ was also performed, which shows similar deep trapped states with anatase TiO₂ (Fig. S8, ESI[†]). It can be speculated that the lack of O₂ evolution for anatase and brookite TiO₂ in the initial stage of the reaction is possibly due to the trapped states that are present in the bulk and surface regions. These states could reduce the overpotential for water oxidation.

Because the photocatalytic performance of anatase TiO₂ changed after long exposure to UV light irradiation, the anatase TiO₂ film was pre-treated under different conditions for TRIRA-EES characterization. As shown in Fig. 5b, the trapped states with their energy levels close to the VB are nearly unchanged after saturated with water vapor, only the integrated densities of states are slightly increased. However, when anatase TiO₂ was treated with UV-laser irradiation, the trapped states were completely removed within the scanning excitation laser wavelength indicating that light irradiation can indeed change the deep trapped states near the VB of anatase TiO₂. Furthermore, we also conducted the Mott–Schottky analysis for all three kinds of TiO₂ before and after the UV light irradiation, indicating that the conduction band (CB) positions were not changed after light treatment (Fig. S9, ESI[†]). From the TRIRA-EES study, we can conclude that the deep trapped states can only be detected for anatase TiO₂ and UV-laser irradiation can remove the deep trapped states, which corresponds to the unique photocatalytic performance for anatase TiO₂.

To confirm the above results, we conducted photocatalytic water oxidation with anatase and rutile TiO₂ pre-treated under UV light irradiation. Anatase and rutile TiO₂ were first irradiated

for different times and then used for water oxidation reactions using AgNO₃ as the electron acceptor. As listed in Table S2 (ESI[†]), anatase TiO₂ shows a remarkable enhancement in O₂ evolution with increasing irradiation time. In fact, the photocatalytic O₂ evolution activity of anatase TiO₂ pre-irradiated for 8 hours is 4 times that of the untreated sample (entries 1–3). However, rutile TiO₂ shows nearly no difference regardless of the irradiation time (entries 4–6). It indicates that the trapped states in anatase TiO₂ can be quenched by light irradiation, consequently resulting in the different performances for water oxidation, which is in good agreement with the TRIRA-EES result.

Based on the above results, we can conclude that the existence of deep trapped states near the VB level of TiO₂ is directly responsible for the POWS behaviors for different phases of TiO₂. A schematic description of deep trapped states for anatase and rutile TiO₂ is shown in Fig. 5c. A plausible explanation is that the deep trapped states located above the VB of anatase TiO₂ can reduce the potential of photogenerated holes that are produced during the photocatalytic reaction. When these trapped states are gradually removed by UV light irradiation, the overpotential for water oxidation is increased and O₂ is produced subsequently. However, the rutile TiO₂ sample does not have trapped states above the VB level, so that it has enough potential to drive the proton reduction and water oxidation reactions even without light treatment. It should be pointed out that the photocatalytic water oxidation on TiO₂ can be ascribed to thermodynamics and kinetics, both of which are closely related but not separated to each other. The presence of deep trapped states near the valence band of anatase and brookite TiO₂ reduce the overpotential for water oxidation, so that the photogenerated holes are more preferable to oxidizing the H₂O molecule to produce the •OH radical. This process is a 2-electron-process, which requires less potential than a 4-electron-process to produce O₂ directly. The UV light irradiation with high intensity can gradually reduce the deep trapped states near the valence band of anatase and brookite TiO₂, so that the overpotential for water oxidation is increased, and simultaneously leads to the result that H₂O can be oxidized by the 4-electron-process to produce O₂.

A DFT calculation was also done to simulate the water oxidation process on anatase, rutile and brookite TiO₂ (Fig. S10, ESI[†]). The adsorption energy of H₂O onto the anatase(101) surface is calculated to be 0.55 eV, and the first O–H dissociation energy is endothermic by 0.34 eV with a barrier of 0.73 eV. As for the product of this step, the H atom is adsorbed onto the O_{2c} atom, and the OH group is left to attach to the Ti_{5c} atom to form a surface-adsorbed hydroxyl radical. The second O–H dissociation step to produce an O atom is predicted to be endothermic by 0.43 eV, with a barrier of 0.62 eV. For the molecular adsorption of water onto the rutile(110) surface, the calculated adsorption energy for H₂O is exothermic by 0.73 eV, and the first O–H dissociation energy is 0.14 eV with a low barrier of 0.23 eV. The second O–H dissociation step is computed to be exothermic by 0.36 eV, with a barrier of 0.45 eV. The calculated adsorption energy for H₂O onto the brookite(210) surface is exothermic by 0.36 eV, and the first O–H dissociation energy is 0.25 eV. All the energies on brookite(210) are larger than that of the rutile(110)

surface, which may be attributed to their different photocatalytic performances. The theoretical calculation results suggest that the water decomposition reaction on the rutile(110) surface is more favorable than that on the anatase(101) and brookite(210) surfaces both thermodynamically and kinetically.

It is worth noting that the surface structures of photocatalysts may be reconstructed under light irradiation. It was reported that anatase TiO₂ will form a disordered layer with two monolayer thickness upon irradiation of high intensity UV light.³⁸ Therefore, it is possible that the surfaces of anatase and brookite TiO₂ may be reconstructed to a quasi-rutile phase surface after prolonged irradiation, which would not only make less trapping states and improve the capability of water oxidation, but also produce more stable and favorable intermediates for the activation of H₂O molecule.

In conclusion, we report that the POWS reaction can take place on rutile but hardly on anatase and brookite TiO₂. However, the POWS on anatase and brookite TiO₂ become feasible under prolonged UV light irradiation. The POWS performances for different phases of TiO₂ are determined by both kinetics and thermodynamics. Kinetically the process of photocatalysis differs on different phases of TiO₂ due to the intermediates (*OH radical for anatase and brookite TiO₂, peroxy species for rutile TiO₂) that are formed. Thermodynamically there are many trapped states lying near the VB of anatase and brookite TiO₂, which reduce the overpotential for water oxidation. These trapped states can be gradually removed by the irradiation of high intensity UV light, such that the POWS reaction can take place finally. Our work will be instructive for understanding the mechanisms for photocatalytic water splitting and shed light on why many semiconductors cannot achieve the POWS despite having thermodynamically suitable band structures for proton reduction and water oxidation reactions.

Acknowledgements

This work was financially supported by the National Natural Science Foundation of China (NSFC Grant No. 21090340) and the 973 National Basic Research Program of the Ministry of Science and Technology (Grant 2014CB239400). The authors would like to thank Prof. James. R. Durrant at ICL for useful discussions.

References

- 1 K. Maeda, T. Takata, M. Hara, N. Saito, Y. Inoue, H. Kobayashi and K. Domen, *J. Am. Chem. Soc.*, 2005, **127**, 8286–8287.
- 2 Y. Ma, X. Wang, Y. Jia, X. Chen, H. Han and C. Li, *Chem. Rev.*, 2014, **114**, 9987–10043.
- 3 R. L. Pozzo, M. A. Baltanas and A. E. Cassano, *Catal. Today*, 1997, **39**, 219–231.
- 4 D. Y. Goswami, *J. Sol. Energy Eng.*, 1997, **119**, 101–107.
- 5 A. L. Linsebigler, G. Lu and J. T. Yates Jr, *Chem. Rev.*, 1995, **95**, 735–758.
- 6 O. Legrini, E. Oliveros and A. Braun, *Chem. Rev.*, 1993, **93**, 671–698.
- 7 A. Fujishima, *Nature*, 1972, **238**, 37–38.
- 8 K. Sayama and H. Arakawa, *J. Chem. Soc., Faraday Trans.*, 1997, **93**, 1647–1654.
- 9 L. Huang, R. Li, R. Chong, G. Liu, J. Han and C. Li, *Catal. Sci. Technol.*, 2014, **4**, 2913–2918.
- 10 K. Maeda, *Chem. Commun.*, 2013, **49**, 8404–8406.
- 11 R. Nakamura, A. Imanishi, K. Murakoshi and Y. Nakato, *J. Am. Chem. Soc.*, 2003, **125**, 7443–7450.
- 12 R. Nakamura and Y. Nakato, *J. Am. Chem. Soc.*, 2004, **126**, 1290–1298.
- 13 R. Nakamura, T. Okamura, N. Ohashi, A. Imanishi and Y. Nakato, *J. Am. Chem. Soc.*, 2005, **127**, 12975–12983.
- 14 P. Salvador, *J. Electrochem. Soc.*, 1981, **128**, 1895–1900.
- 15 P. Salvador, *J. Phys. Chem. C*, 2007, **111**, 17038–17043.
- 16 P. Salvador and C. Gutierrez, *J. Phys. Chem.*, 1984, **88**, 3696–3698.
- 17 Y. Nosaka, S. Komori, K. Yawata, T. Hirakawa and A. Y. Nosaka, *Phys. Chem. Chem. Phys.*, 2003, **5**, 4731–4735.
- 18 A. Valdes, Z.-W. Qu, G.-J. Kroes, J. Rossmeisl and J. K. Nørskov, *J. Phys. Chem. C*, 2008, **112**, 9872–9879.
- 19 M. Lazzeri, A. Vittadini and A. Selloni, *Phys. Rev. B: Condens. Matter Mater. Phys.*, 2001, **63**, 155409.
- 20 H. Perron, C. Domain, J. Roques, R. Drot, E. Simoni and H. Catalette, *Theor. Chem. Acc.*, 2007, **117**, 565–574.
- 21 R. Chong, J. Li, X. Zhou, Y. Ma, J. Yang, L. Huang, H. Han, F. Zhang and C. Li, *Chem. Commun.*, 2013, **49**, 165–167.
- 22 H. Lin, L. Li, M. Zhao, X. Huang, X. Chen, G. Li and R. Yu, *J. Am. Chem. Soc.*, 2012, **134**, 8328–8331.
- 23 K. Maeda, *Chem. Commun.*, 2013, **49**, 8404–8406.
- 24 G. Liu, H. G. Yang, J. Pan, Y. Q. Yang, G. Q. Lu and H.-M. Cheng, *Chem. Rev.*, 2014, **114**, 9559–9612.
- 25 T. Hirakawa and Y. Nosaka, *Langmuir*, 2002, **18**, 3247–3254.
- 26 V. Brezova, D. Dvoranova and A. Staško, *Res. Chem. Intermed.*, 2007, **33**, 251–268.
- 27 F. A. Villamena, J. K. Merle, C. M. Hadad and J. L. Zweier, *J. Phys. Chem. A*, 2005, **109**, 6089–6098.
- 28 J. Yu, J. Chen, C. Li, X. Wang, B. Zhang and H. Ding, *J. Phys. Chem. B*, 2004, **108**, 2781–2783.
- 29 X. Yang, C. Salzmann, H. Shi, H. Wang, M. L. Green and T. Xiao, *J. Phys. Chem. A*, 2008, **112**, 10784–10789.
- 30 R. Li, H. Kobayashi, J. Guo and J. Fan, *Chem. Commun.*, 2011, **47**, 8584–8586.
- 31 T. Berger, M. Sterrer, O. Diwald, E. Knözinger, D. Panayotov, T. Thompson and J. Yates, *J. Phys. Chem. B*, 2005, **109**, 6061–6068.
- 32 D. C. Hurum, A. G. Agrios, K. A. Gray, T. Rajh and M. C. Thurnauer, *J. Phys. Chem. B*, 2003, **107**, 4545–4549.
- 33 F. Zuo, L. Wang, T. Wu, Z. Zhang, D. Borchardt and P. Feng, *J. Am. Chem. Soc.*, 2010, **132**, 11856–11857.
- 34 K. Suriye, P. Praserttham and B. Jongsomjit, *Appl. Surf. Sci.*, 2007, **253**, 3849–3855.
- 35 M. Zhu, Y. Mi, G. Zhu, D. Li, Y. Wang and Y. Weng, *J. Phys. Chem. C*, 2013, **117**, 18863–18869.
- 36 Y. Mi and Y. Weng, *Sci. Rep.*, 2015, **5**, 11482, DOI: 10.1038/srep11482.
- 37 I. Mora-Seró and J. Bisquert, *Nano Lett.*, 2003, **3**, 945–949.
- 38 L. Zhang, B. K. Miller and P. A. Crozier, *Nano Lett.*, 2013, **13**, 679–684.